LIDAR SYSTEM CALIBRATION USING OVERLAPPING STRIPS

Calibração do sistema LiDAR utilizando faixas sobrepostas

KI IN BANG [1]
AYMAN F. HABIB [1]
MAURICIO MÜLLER [2]

[1] Dept. of Geomatics Engineering, University of Calgary, 2500 University Drive NW, Calgary, AB, T2N 1N4, Canada
email: {kibang, ahbib}@ucalgary.ca
[2] LACTEC – Institute of Technology for the Development, Centro Politécnico da UFPR, Caixa Postal - 19067 - CEP: 81531-980, Jardim das Américas - Curitiba - Paraná – Brasil
email: muller@lactec.org.br

ABSTRACT

A LiDAR system calibration procedure estimates a set of parameters that represent biases in the system parameters and measurements. These parameters can be used to improve the quality of any subsequently-collected LiDAR data. Current LiDAR calibration techniques require full access to the system parameters and raw measurements (e.g., platform position and orientation, laser ranges, and scan-mirror angles). Unfortunately, the raw measurements are not usually available to end-users. The absence of such information is limiting the widespread adoption of LiDAR calibration activities by the end users. This research proposes alternative methods for LiDAR system calibration, without the need for the system raw measurements. The simplified method that is proposed in this paper uses the available coordinates of the LiDAR points in overlapping parallel strips to estimate biases in the system parameters and measurements (more specifically, biases in the planimetric lever-arm offset components, boresight angles, ranges, and mirror-angles). In this approach, the conventional LiDAR equation is simplified based on a few reasonable assumptions; the simplified LiDAR equation is then used to model the mathematical relationship between conjugate surface elements in overlapping

parallel strips in the presence of the systematic biases. In addition, a quasi-rigorous calibration method is also proposed to deal with non-parallel overlapping strips. The quasi-rigorous method can handle heading angle and elevation variations of platform trajectories since it also makes use of time-tagged point cloud and trajectory position data. To illustrate the feasibility and the performance of the proposed calibration methods, experimental results from simulated and real datasets are introduced.
Keywords: LiDAR; Laser Scanning; Calibration; Geo-ferencing; Accuracy.

1. INTRODUCTION

A typical LiDAR system consists of a laser ranging and scanning unit together with a Position and Orientation System (POS), which encompasses an integrated Differential Global Positioning System (DGPS) and an Inertial Navigation System (INS). A laser scanner mounted on the platform scans object surfaces and produces a wide swath over which the distance to an object is measured. The angle at which the laser is scanned is measured. To correct for the platform's movement, the motion of the platform is recorded by the GPS/INS navigation system and the information is used in a post-processing mode. The fundamentals and detailed principles of the laser ranging operation was well documented by Baltsavias (1999); Wehr and Lohr (1999), and the common method to determine the coordinates of LiDAR footprints was fully explained by Vaughn et al. (1996).

The accuracy of LiDAR products is relatively high (vertical: 5-30 cm, horizontal: about 80cm), and the quality of the LiDAR data is affected by many factors: a) position and attitude measurement quality, b) system calibration quality, and c) flying height and speed (McGlone, 2004). The coordinates of the LiDAR footprints are the result of combining the derived measurements from each of its system components, as well as the mounting parameters relating such components. The relationship between the system measurements and parameters is embodied in the LiDAR equation (Vaughn et al., 1996 and Schenk, 2001), Equation 1.

The position of the LiDAR footprint, $\vec{X}_G$, can be derived through the summation of three vectors ($\vec{X}_0$, $\vec{P}_G$ and $\vec{\rho}$) after applying the appropriate rotations: $R_{yaw,pitch,roll}$, $R_{\Delta\omega\Delta\varphi\Delta\kappa}$, and $R_{\alpha\beta}$. In Equation 1, $\vec{X}_0$ is the vector between the origins of the ground and the Inertial Measurement Unit (IMU) body frame, $\vec{P}_G$ is the offset between the laser unit frame and the IMU body frame (lever-arm offset), and $\vec{\rho}$ is the laser range vector whose magnitude is equivalent to the distance from the laser firing point to its footprint. The term $R_{yaw,pitch,roll}$ stands for the rotation matrix relating the ground and IMU body frame, $R_{\Delta\omega\Delta\varphi\Delta\kappa}$ represents the rotation matrix relating the IMU and laser unit frame (boresight matrix), and $R_{\alpha\beta}$ refers to the rotation matrix relating the laser unit frame and laser beam frame with α and β

being the mirror scan angles. For a linear scanner, which is the focus of this paper, the mirror is rotated in one direction only (i.e., α is equal to zero).

$$\vec{X}_G = \vec{X}_0 + R_{yaw,\ pitch,\ roll}\left(\vec{P}_G + R_{\Delta\omega,\ \Delta\phi,\ \Delta\kappa} R_{\alpha,\ \beta}\begin{bmatrix} 0 \\ 0 \\ -\rho \end{bmatrix}\right) \tag{1}$$

The involved quantities in the LiDAR equation are all measured during the acquisition process except for the lever-arm offset and boresight angles, which are usually determined through a calibration procedure. To make sure that the LiDAR data meets the required and predicted quality, LiDAR system calibration has been investigated in many ways, and conventional calibration methods have been carried out based on system raw measurements and LiDAR equation. Schenk (2001) introduced the sources of systematic errors that can occur in a LiDAR system, and a calibration procedure was then proposed based on such an analysis. This work comprehensively explained possible errors in a LiDAR system, but it seems too complex in terms of an effective calibration procedure. Furthermore, all introduced calibration parameters were not solved for simultaneously due to their correlations; for example, biases in the scanner mirror angles and laser scanner mounting errors.

The calibration procedure introduced by Morin (2002) solves for the boresight angles and the scanner torsion. These parameters are either estimated using ground control points or by manually observing discrepancies between tie points in overlapping strips. The drawback of this approach is that the identification of distinct control and tie points in LiDAR data is a difficult task due to the irregular and sparse nature of the collected point cloud.

Skaloud and Lichti (2006) presented a calibration technique using tie planar patches in overlapping strips. The underlying assumption of this procedure is that systematic errors in the LiDAR system will lead to non-coplanarity of conjugate planar patches as well as bending effects in these patches. The calibration method uses the LiDAR equation to simultaneously solve for the plane parameters as well as the boresight angles and a bias in laser ranges. However, this approach requires relatively large planar patches, which might not always be available, especially in rural areas.

According to Habib et al. (2007), when the lever-arm offset and boresight angles are considered at the same time, one of the difficulties is the correlations between these parameters. Therefore, the use of planar patches should be carefully handled through the use of an optimal flight plan, as well as optimal planar patch distribution due to the correlations between these calibration parameters (Habib et al., 2007).

Since Ackermann (1999) introduced the potential integration of imaging and laser sensors, research has been performed to investigate the potential and limitations of the integration of LiDAR and photogrammetric data. For example, Postolov et al. (1999) and Ghanma (2006) introduced the co-registration between LiDAR and photogrammetric data, and Bretar (2004) generated a DSM from photogrammetric data which was then compared with LiDAR data for the strip adjustment. Habib et al. (2007) used planar patches derived from photogrammetric data for LiDAR system calibration, where the photogrammetric bundle adjustment was augmented by adding the LiDAR equation to the collinearity equations using the LiDAR system raw measurements.

This paper introduces two approximate methods for the LiDAR system calibration: a simplified method using overlapping strips without system raw measurements, and a quasi-rigorous method using time-tagged laser footprint coordinates of overlapping strips and trajectory positions. In these methods, the discrepancies between overlapping strips are utilized to determine the correction terms to the initial calibration parameters. In the next section, we will discuss how to modify the LiDAR equation for the simplified method and the utilization of the time-tagged point cloud and trajectory positions for the quasi-rigorous method. Then, experiment results from simulated and real datasets are presented. Finally, the manuscript summarizes its conclusions and recommendations for future works.

2. PROPOSED METHODS

The LiDAR system calibration considers the alignment of integrated sensors and the systematic errors in a laser scanner. A rigorous calibration method is commonly carried out using system raw measurements (from GPS/INS and laser scanner) and the conventional LiDAR equation (refer to Equation 1). This paper introduces new methods, where system raw measurements are not required and the biases in the system parameters are determined using overlapping strips. The simplified method using only point cloud coordinates consists of two steps: 1) determination of discrepancies between parallel overlapping strips through a conventional 3D transformation procedure, and 2) estimation of biases in system parameters from the obtained transformation parameters. Another proposed method, the quasi-rigorous method, can handle non-parallel overlapping strips using time-tagged point cloud coordinates and trajectory position data. In this method, time information is utilized to rigorously determine the locations of the firing points for laser footprints.

2.1 Simplified method

Discrepancies among overlapping strips occur if LiDAR footprints are generated by incorrect system parameters. The new proposed method detects and

evaluates the discrepancies between overlapping strips using the conventional 3D transformation procedure. The result of this procedure is represented by transformation parameters: rotation angles and shifts. Then, the proposed method estimates correction terms of the LiDAR system parameters using the transformation parameters. The key issue of this methodology is defining the relationship between the transformation parameters and LiDAR system parameters. In order to establish the relationship, we simplify the conventional LiDAR equation. For the mathematical derivation of the simplified LiDAR equation, a few reasonable assumptions are considered regarding the platform trajectory and the object surface: i) linear scanning systems are considered, ii) the object surface is nearly flat in comparison to the flying height, iii) the flight lines are parallel, iv) the platform trajectory is straight, v) the roll and pitch angles of the platform are zero, and vi) the boresight angles are considered as very small angles.

The simplified method works with an additional coordinate system which is defined within the overlapping area. Its *Y*-axis is parallel and halfway between the flight lines, Figure 1. The positive direction of the *Y*-axis indicates the forward flight direction, and the *X* axis is along the scan line (across the flight direction). In the figure, x_A and x_B denote lateral coordinates of a ground object point, *P*, w.r.t. the laser unit frames for the forward and backward flights, respectively; the lateral distance between two flight lines is represented by D_x.

Using the above assumptions and the user defined coordinate system, the original LiDAR equation can be approximated by Equation 2. In this equation, ΔX, ΔY, ΔZ, $\Delta\omega$, $\Delta\varphi$, and $\Delta\kappa$ denote the lever-arm offset and boresight angles, *S* is the scale factor of the scan angles, and ρ is the laser range. The laser unit frame coordinate *x* and flying height *H* are the same as the terms $-\rho\sin(\beta S)$ and $\rho\cos(\beta S)$ in Equation 2. The multiple signs ($\pm$ & $\mp$) indicate two parallel strips with the upper sign referring to the forward strip, while the lower sign referring to the backward strip.

The impact of the systematic errors is represented in terms of the system parameters in Equation 3; $\bar{X}_{True}$ is the error-free coordinates, while $\bar{X}_{Biased}$ denotes the derived laser footprint coordinate which may be distorted by biases ($\delta\bar{x}$) in the system parameters. The impacts of biases in lever-arm offset, boresight angles, laser range, and scan angle scale are introduced in the second line of Equation 3, in detail. These error terms are derived through the partial derivatives of Equation 2 w.r.t. the considered calibration parameters, after ignoring second and higher order bias terms.

Figure 1 - Flight lines and definitions of the used coordinate systems in parallel overlapping strips

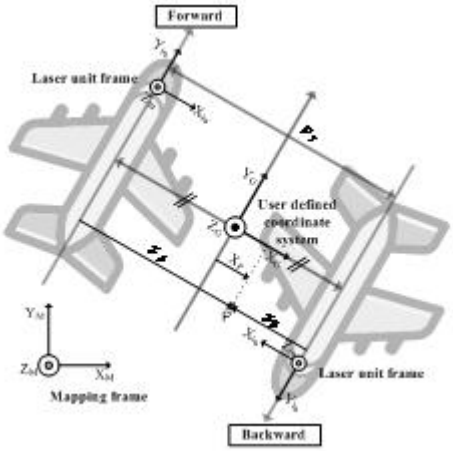

$$\vec{X}_G \approx \vec{X}_0 + \begin{bmatrix} \pm\Delta X \\ \pm\Delta Y \\ \Delta Z \end{bmatrix} + \begin{bmatrix} \pm 1 & \mp\Delta\kappa & \pm\Delta\phi \\ \pm\Delta\kappa & \pm 1 & \mp\Delta\omega \\ -\Delta\phi & \Delta\omega & 1 \end{bmatrix} \begin{bmatrix} -\rho\sin(S\beta) \\ 0 \\ -\rho\cos(S\beta) \end{bmatrix} \tag{2}$$

$$\vec{X}_{Biased} \approx \vec{X}_{True} + \frac{\partial f}{\partial \vec{x}}\delta\vec{x}$$

$$= \vec{X}_{True} + \underbrace{\begin{bmatrix} \pm\delta\Delta X \\ \pm\delta\Delta Y \\ \delta\Delta Z \end{bmatrix}}_{lever-arm\ offset} + \underbrace{\begin{bmatrix} \mp H\delta\Delta\phi \\ \pm x\delta\Delta\kappa \pm H\delta\Delta\omega \\ -x\delta\Delta\phi \end{bmatrix}}_{boresighting\ angles} + \underbrace{\begin{bmatrix} \mp\sin(S\beta)\delta\rho \\ 0 \\ -\cos(S\beta)\delta\rho \end{bmatrix}}_{range\ bias} + \underbrace{\begin{bmatrix} \mp H\beta\delta S \\ 0 \\ -x\beta\delta S \end{bmatrix}}_{scale\ factor} \tag{3}$$

For overlapping strips, the discrepancies between two strips can be considered as the accumulated impact of the systematic errors on these strips; it is mathematically represented in Equation 4. To determine all the biases in the system parameters, except for $\delta\Delta Z$, two kinds of overlapping strip pairs are considered: case 1 consist of overlapping strips captured with 100% overlap ratio and opposite flight directions (forward and backward), and case 2 consists of overlapping strips captured with less than 100% overlap ratio and the same flight direction (Figure 2).

$$\vec{X}^{A}_{Biased} - \vec{X}^{B}_{Biased} \approx \left(\frac{\partial f^{A}}{\partial \vec{x}} - \frac{\partial f^{B}}{\partial \vec{x}} \right) \delta\vec{x} \tag{4}$$

Figure 2 - Two overlapping cases are specified to de-couple involved calibration parameters

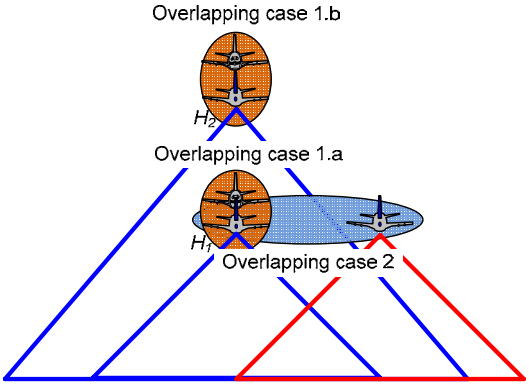

Equations 5.a and 5.b show the final forms for cases 1 and 2, respectively. As shown in Equation 5.a, case 1 (opposite directions and 100% overlap ratio) can be used to solve for the system biases, $\delta\Delta X$, $\delta\Delta Y$, $\delta\Delta\omega$, and $\delta\Delta\varphi$, while case 2 (same direction and less than 100% overlap ratio) contribute to the estimation of $\delta\rho$, δS, $\delta\Delta\varphi$, and $\delta\Delta\kappa$. After re-parameterization, we can notice that the forms of Equations 5.a and 5.b are similar to the conventional 3D transformation function with 4 parameters: three shifts and one rotation around Y axis (roll angle). An additional observation that has surfaced from this procedure is that the 4-parameter transformation is appropriate for the strip adjustment while considering the system biases ($\delta\Delta X$, $\delta\Delta Y$, $\delta\Delta\omega$, $\delta\Delta\varphi$, $\delta\Delta\kappa$, $\delta\rho$, and δS) introduced in this paper.

To use this simplified method, one should note two facts. The first, $\delta\Delta Z$, the bias in the lever-arm offset along the Z direction, cannot be estimated in this procedure because overlapping strips do not have any discrepancy caused by this bias regardless of the flight direction, flying height, or scan mirror angle. The second, two different flying heights (see cases 1.a and 1.b in Figure 2) are required to de-couple $\delta\Delta Y$ and $\delta\Delta\omega$; as we can see in Equation 5.a, $\delta\Delta Y$ and $\delta\Delta\omega$ are coupled together. Using two flying heights, one can solve this problem since the impact of $\delta\Delta Y$ is independent of the flying height; however, $\delta\Delta\omega$ produces different errors as the flying height changes.

$$\vec{X}_G^{A'} = \underbrace{\begin{bmatrix} 2\delta\Delta X - 2H\delta\Delta\phi \\ 2\delta\Delta Y + 2H\delta\Delta\omega \\ 0 \end{bmatrix}}_{shifts} + \underbrace{R_{2\delta\Delta\phi}}_{roll} \vec{X}_G^{B'} \qquad (5.a)$$

$$\vec{X}_G^{A'} = \underbrace{\begin{bmatrix} \frac{D_X}{H}\delta\rho + D_X\delta S \\ D_X\delta\Delta\kappa \\ -D_X\delta\Delta\phi \end{bmatrix}}_{shifts} + \underbrace{R_{\frac{-2D_X}{H}\delta S}}_{roll}\vec{X}_G^{B'} \tag{5.b}$$

2.2 Quasi-rigorous method

The quasi-rigorous method can deal with non-parallel strips. In addition, this method can handle heading variation and varying elevations since it makes use of time-tagged point cloud and trajectory position data. In other words, this method is developed under the following assumptions: a) we are dealing with a linear scanner, b) the LiDAR system is almost vertical (i.e., pitch and roll angles are close zero), and c) the LiDAR system has relatively small boresight angles. Such assumptions simplify the LiDAR geometric model as represented by Equation 1 to the form in Equation 6.

$$\begin{aligned} \vec{X}_G \approx \vec{X}_o + \begin{bmatrix} \cos\kappa & -\sin\kappa & 0 \\ \sin\kappa & \cos\kappa & 0 \\ 0 & 0 & 1 \end{bmatrix}\begin{bmatrix} \Delta X \\ \Delta Y \\ \Delta Z \end{bmatrix} \\ + \begin{bmatrix} \cos\kappa & -\sin\kappa & 0 \\ \sin\kappa & \cos\kappa & 0 \\ 0 & 0 & 1 \end{bmatrix}\begin{bmatrix} 1 & -\Delta\kappa & \Delta\varphi \\ \Delta\kappa & 1 & -\Delta\omega \\ -\Delta\varphi & \Delta\omega & 1 \end{bmatrix}\begin{bmatrix} x \\ 0 \\ z \end{bmatrix} \end{aligned} \tag{6}$$

The difference between Equations 6 and 2 (which is derived for the simplified method) is the additional rotation matrix defined by the heading angle, κ. The quasi-rigorous method is developed for handling general flight lines, which means that the trajectory is not limited to a straight line. The platform positions are available from the trajectory position data, which is linked to the time-tagged point cloud coordinates. Therefore, the location of the firing point corresponding to each LiDAR point can be estimated. In Equation 6, x and z are the coordinates of the LiDAR point with respect to the laser unit frame (refer to Figure 1); those are approximately estimated by the firing point and LiDAR point coordinates. The coordinate z is the elevation difference between the firing point and LiDAR point. As shown in Figure 3, the coordinate x represents the lateral distance between the LiDAR point in question and the projection of the flight trajectory onto the ground. The trajectory line for a given LiDAR point is determined by a line-fitting

procedure using several trajectory positions at the vicinity of the time associated with the point in question.

Figure 3 - Lateral distance between the LiDAR point in question and the projection of the flight trajectory onto the ground

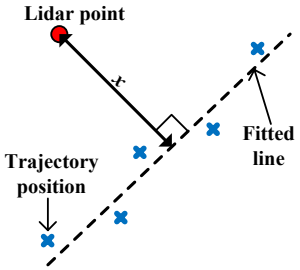

In the presence of biases in the system parameters, Equation 7 shows the biased LiDAR point coordinates, $\vec{X}_{Biased}$, which is a function of the system parameters, $\vec{x}$, the biases in the system parameters, $\delta\vec{x}$, and the measurements, $\vec{l}$. Equation 7 can be linearized with respect to the system parameters using Taylor series expansion to get the form in Equation 8, after ignoring second and higher order terms.

$$\vec{X}_{Biased} = f(\vec{x} + \delta\vec{x}, \vec{l}) \tag{7}$$

$$\begin{aligned} \vec{X}_{Biased} &\approx f(\vec{x}, \vec{l}) + \frac{\partial f}{\partial \vec{x}}\delta\vec{x} = \vec{X}_{True} + \frac{\partial f}{\partial \vec{x}}\delta\vec{x} = \vec{X}_{True} + \begin{bmatrix} \delta X_G \\ \delta Y_G \\ \delta Z_G \end{bmatrix} \\ &= \vec{X}_{True} + \begin{bmatrix} \delta X_G \\ \delta Y_G \\ \delta Z_G \end{bmatrix}_{\delta\Delta X, \delta\Delta Y, \delta\Delta Z} + \begin{bmatrix} \delta X_G \\ \delta Y_G \\ \delta Z_G \end{bmatrix}_{\delta\Delta\omega, \delta\Delta\varphi, \delta\Delta\kappa} + \begin{bmatrix} \delta X_G \\ \delta Y_G \\ \delta Z_G \end{bmatrix}_{\delta\rho} + \begin{bmatrix} \delta X_G \\ \delta Y_G \\ \delta Z_G \end{bmatrix}_{\delta S} \end{aligned} \tag{8}$$

Due to the presence of various systematic errors, the bias-contaminated coordinates of conjugate points in overlapping strips will show systematic discrepancies. The mathematical relationship between these points can be derived by rewriting Equation 8 for two overlapping strips (A and B) and subtracting the resulting equations from each other. Such a relationship is shown in Equation 9.

$$\begin{bmatrix} X_A \\ Y_A \\ Z_A \end{bmatrix}_{Biased} - \begin{bmatrix} X_B \\ Y_B \\ Z_B \end{bmatrix}_{Biased} = \begin{bmatrix} (\cos\kappa_A - \cos\kappa_B)\delta\Delta X - (\sin\kappa_A - \sin\kappa_B)\delta\Delta Y \\ (\sin\kappa_A - \sin\kappa_B)\delta\Delta X + (\cos\kappa_A - \cos\kappa_B)\delta\Delta Y \\ 0 \end{bmatrix} +$$
$$+ \begin{bmatrix} (\sin\kappa_A z_A - \sin\kappa_B z_B)\delta\Delta\omega + (\cos\kappa_A z_A - \cos\kappa_B z_B)\delta\Delta\phi - (\sin\kappa_A x_A - \sin\kappa_B x_B)\delta\Delta\kappa \\ -(\cos\kappa_A z_A - \cos\kappa_B z_B)\delta\Delta\omega + (\sin\kappa_A z_A - \sin\kappa_B z_B)\delta\Delta\phi(\cos\kappa_A x_A - \cos\kappa_B x_B)\delta\Delta\kappa \\ -(x_A - x_B)\delta\Delta\phi \end{bmatrix} + \quad (9)$$
$$+ \begin{bmatrix} -[\cos\kappa_A \sin(S\beta_A) - \cos\kappa_B \sin(S\beta_B)]\delta\rho + (\cos\kappa_A z_A \beta_A - \cos\kappa_B z_B \beta_B)\delta S \\ -[\sin\kappa_A \sin(S\beta_A) - \sin\kappa_B \sin(S\beta_B)]\delta\rho + (\sin\kappa_A z_A \beta_A - \sin\kappa_B z_B \beta_B)\delta S \\ -[\cos(S\beta_A) - \cos(S\beta_B)]\delta\rho - (x_A \beta_A - x_B \beta_B)\delta S \end{bmatrix}$$

Equation 9 is the final linear observation equations when dealing with overlapping strips in the quasi-rigorous method. These equations allow us to recover the biases in the system parameters. It should be noted that, when using only overlapping strips, the bias in the lever-arm offset along the *Z* direction ($\delta\Delta Z$) cannot be estimated. Such inability is caused by the fact that a vertical bias in the lever-arm offset parameters produces the same effect regardless of the flight direction, flying height, or scan mirror angle. When vertical control data over flat horizontal surface is also employed, we cannot recover $\delta\Delta Z$ and $\delta\rho$ simultaneously due to the high correlation between these parameters. This type of control data will only contribute for the estimation of the roll ($\delta\Delta\varphi$), the range bias ($\delta\rho$) and the mirror angle scale biases (δS). The use of full control data over sloped surfaces will contribute for the estimation of all parameters and might help decoupling $\delta\Delta Z$ and $\delta\rho$. Equation 10 shows the form derived for control data use. This equation can be also used to correct the biased LiDAR point cloud after estimating the error terms in the system parameters. In this case, the left-hand side represents the corrected coordinates calculated using the given coordinates and estimated parameters.

One should note that the mathematical models for the simplified and the quasi-rigorous calibration methods are derived based on a point primitive (i.e., conjugate points in overlapping strips). However, it is known that point correspondence is not available in point cloud data. For this reason, linear features and planar patches have been alternatively used as conjugate surface elements in overlapping strips (Lee et al., 2007; Habib and et al., 2007). In this research, however, the Iterative Closest Patch (ICPatch) procedure is applied to establish correspondence between two overlapping strips using conjugate point and TIN patch pairs. For more information regarding the ICPatch method and how it can be used to estimate descripancies between overlapping strips, interested readers can refer to Habib et al., 2006 and Bang et al., 2008.

$$\begin{bmatrix} X_C \\ Y_C \\ Z_C \end{bmatrix}_{Control} = \begin{bmatrix} X \\ Y \\ Z \end{bmatrix}_{LiDAR} - \begin{bmatrix} \cos\kappa\,\delta\Delta X - \sin\kappa\,\delta\Delta Y + \sin\kappa\, z\,\delta\Delta\omega + \cos\kappa\, z\,\delta\Delta\phi \\ \sin\kappa\,\delta\Delta X + \cos\kappa\,\delta\Delta Y - c\cos\kappa\, z\,\delta\Delta\omega + \sin\kappa\, z\,\delta\Delta\phi \\ -x\,\delta\Delta\phi \end{bmatrix} - \begin{bmatrix} -\sin\kappa\, x\,\delta\Delta\kappa - \cos\kappa\sin(S\beta)\,\delta\rho + c\cos\kappa\, z\,\beta\,\delta S \\ \cos\kappa\, x\,\delta\Delta\kappa - \sin\kappa\sin(S\beta)\,\delta\rho + s\sin\kappa\, z\,\beta\,\delta S \\ -\cos(S\beta)\,\delta\rho - x\,\beta\,\delta S \end{bmatrix} \quad (10)$$

3. EXPERIMENTS

In this section, feasibility tests for the proposed calibration methods using simulated and real datasets are represented. The main purpose of utilizing simulated data for the experiments is to verify the performance of the proposed models in a controlled environment. In addition, we can verify the impact of deviations from the listed assumptions previously mentioned.

3.1 Simulated datasets

The simulated data was produced using a LiDAR system with a pulse repetition rate of 167 kHz, a scan rate of 100 Hz, and a scan angle variation from -22° to +22°. Six strips in three overlapping pairs are simulated (see Table 1 and Figure 4). Strips 1 and 2 are captured from a flying height of 1,000m in opposite directions with 100% overlap ratio. Strips 3 and 4 captured from a 2,500m flying height with 50% overlap ratio and in the same flight directions. Strips 5 and 6 are flown at 2,000m flying height with 100% overlap ratio and opposite flight directions. This testing configuration allows the maximization of the impact of systematic biases and has the ability to de-couple the different biases from each other. For testing the impact of deviations from the underlying assumptions, three cases are designed in terms of the parallelism of the flight lines. In Table 1, one can see that three overlapping cases are simulated. In the first case, overlapping strips are parallel to each other; in the second case, overlapping strips are non-parallel to each other with 10° deviation; in the third case, the degree of the non-parallelism is 30° (see the flying directions in Table 1). As it can be seen in Figure 4, the simulated surface has various planar patches with well distributed aspects. The heights in the simulated surface are in the range [0.0 – 112.5m]. Using the simulated surface and flight-line trajectories, the LiDAR measurements were derived. Then, biases were introduced to the system parameters (the magnitudes of these biases are listed in Table 2).

Table 1 - 6 strips are simulated with one parallel and two non-parallel overlapping cases

Strips	Flying direction [°]			Flying height [m]
	Case 1 Parallel	Case 2 10° non-parallel	Case 3 30° non-parallel	
1	0	5	15	1,000
2	180	175	165	1,000
3	0	5	15	2,500
4	0	-5	-15	2,500
5	0	5	15	2,000
6	180	175	165	2,000

Figure 4 - Illustration of the simulated surface and flight lines

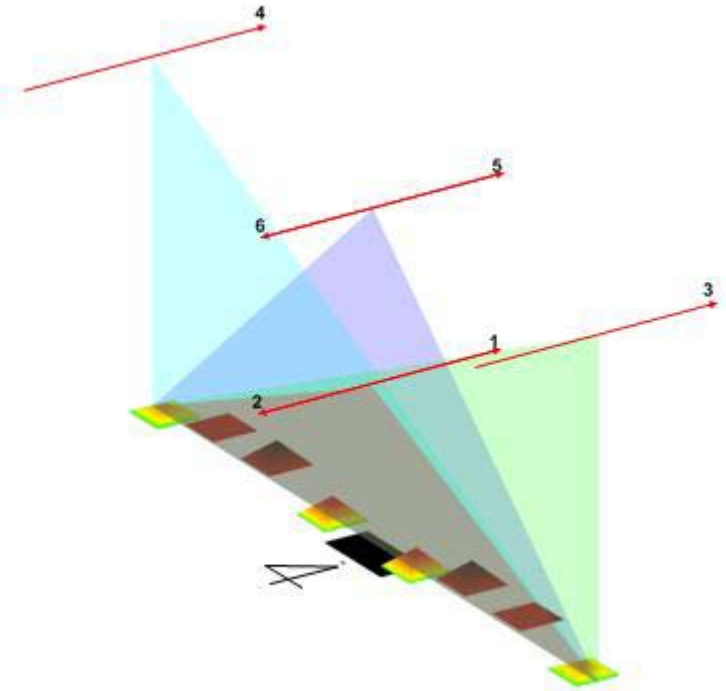

Table 2 -. Systematic biases intentionally added to the system parameters

δΔX (m)	δΔY (m)	δΔZ (m)	δΔω (deg)	δΔφ (deg)	δΔκ (deg)	Δρ (m)	δS
0.05	0.05	0.05	0.01	0.01	0.01	0.5	0.001

As it is mentioned earlier, the simplified method consists of a two-step procedure. First, the discrepancies between overlapping strips are evaluated using a 3D transformation; second, the system biases are estimated from the estimated parameters. The transformation parameters (w.r.t. the local coordinate system) for the simulated overlapping strips are shown in Table 3. It should be noted that only the 3D shifts and the roll angle (φ) across the flight direction are used for the estimation of biases in the system parameters according to the simplified calibration procedure. The deviations of the estimated pitch and heading angles (ω and κ) from zeros can be used to indicate the presence of additional biases beyond what is considered in this manuscript. Moreover, the pitch and heading angles would also indicate any deviation from the underlying assumptions (e.g., non-parallel strips). As it can be seen in Table 3 – case 1, the estimated pitch and heading angles of the 3D transformation parameters are quite small. On the other hand, the estimated heading angles for cases 2 and 3 show the impact of dealing with non-parallel strips.

Table 3 - Estimated 3D Transformation parameters w.r.t. the local coordinate system between the simulated strips, whose specifications are shown in Table 1

Case	Strips	X_T(m)	Y_T(m)	Z_T(m)	ω(deg)	φ(deg)	κ(deg)
(1) parallel	1&2	-0.23	0.42	0.00	0.004	0.020	0.001
	4&3	-1.42	-0.20	0.23	-0.004	0.058	-0.001
	5&6	-0.58	0.78	0.00	0.002	0.020	0.001
(2) 10°	1&2	-0.24	0.42	0.00	0.001	0.021	0.038
	4&3	-1.47	-0.30	0.26	0.001	0.057	0.014
	5&6	-0.58	0.76	0.00	-0.003	0.021	0.041
(3) 30°	1&2	-0.23	-0.41	-0.00	0.002	0.019	0.045
	4&3	-1.54	-0.39	0.22	-0.003	0.054	0.034
	5&6	-0.54	0.75	-0.00	0.003	0.018	0.037

Table 4 presents the biases in the system parameters which are estimated from the determined transformation parameters in Table 3 based on Equations 5.a and 5.b Comparing Tables 2 and 4, one can see that the estimated biases are quite close to the introduced biases. We can also observe in Table 4 that the non-parallelism of the flight lines mainly affected the heading bias. Although we see some deviation, we can say that the estimated biases are quite close to the real ones, which indicate the validity of the proposed simplified method for scenarios with reasonable deviations from the listed assumptions.

In the LiDAR simulation procedure, the platform trajectory positions are recorded for the quasi-rigorous method tests. Table 5 represents the biases in the system parameters estimated by the quasi-rigorous method. Those estimated parameters are very close to the parameters introduced in the simulated datasets and

are quite better compared to the results from the simplified method, especially for the non-parallel strips. As shown in Table 5, the estimated parameters are relatively consistent in all three cases. From these results, we can verify that the quasi-rigorous method accurately estimates the systematic biases regardless of the flight direction deviations. This performance is not a surprise since the quasi-rigorous method can handle non-parallel strips with varying heading. Such strength enables the quasi-rigorous method to be widely applied to general overlapping strips.

Table 4 - Biases in the system parameters estimated by the simplified method from the transformation parameters (three shifts and roll angle) presented in Table 3

Case	δΔX (m)	δΔY (m)	δΔω (deg)	δΔφ (deg)	δΔκ (deg)	Δρ (m)	δS
1	0.05	0.04	0.0103	0.0100	0.0095	0.37	0.0011
2	0.06	0.05	0.0097	0.0105	0.0143	0.52	0.0011
3	0.05	0.05	0.0096	0.0094	0.0189	0.83	0.0009

Table 5 - Biases in the system parameters estimated by the quasi-rigorous method

Case	δΔX (m)	δΔY (m)	δΔω (deg)	δΔφ (deg)	δΔκ (deg)	Δρ (m)	δS
1	0.05	0.05	0.0099	0.0100	0.0089	0.48	0.0010
2	0.05	0.05	0.0101	0.0100	0.0096	0.50	0.0009
3	0.05	0.05	0.0100	0.0100	0.0096	0.53	0.0010

3.2 Real datasets

To evaluate the performance of the proposed methodology, a LiDAR dataset, which was captured by an Optech ALTM 2050 using the optimum flight configuration, was utilized. In addition to strips in the optimum configuration, some extra strips were acquired as well. In Figure 5, strips 1, 2, and 6 are captured from 2,000m flying height; the other strips have 1,000m flying height. When it comes to the flight directions, strips 1, 3, 5, and 8 are flown from SW to NE; the other strip are from NE to SW. Table 6 presents the seven overlapping strip pairs configured for the proposed methods.

Table 7 shows the transformation parameters (w.r.t. the local coordinate system) prepared for the simplified method, and the estimated system biases determined from the transformation parameters are reported in Table 8. In Table 7, we can see that the estimated heading angles show some deviation from the expected zero value. Such deviation can be attributed to possible navigation errors and the non-parallelism of the flight lines.

For the quasi-rigorous method, two conditions are tested: 1) using only overlapping strip pairs and 2) using overlapping strip pairs together with a control surface, which consists of 900 points observed by GPS surveying over the airport runway. Table 9 shows the biases estimated by the quasi-rigorous method using only overlapping strip pairs; Table 10 reports the result using the overlapping strip pairs and the control surface. The significant difference between the two tests is observed in the estimates of $\Delta\rho$ and δS. Such a difference is due to the correlation between these two parameters, which can be de-coupled using control data.

Figure 5 - Illustration of the 8 strip configuration of the real dataset

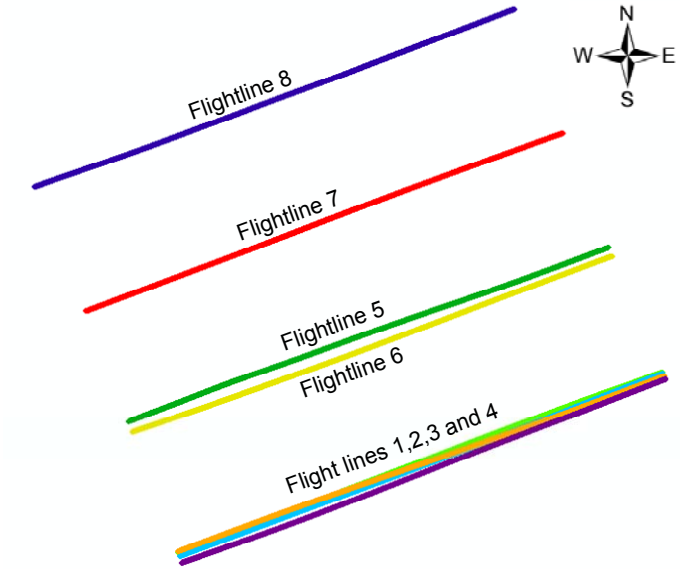

Table 6 - 7 overlapping strip pairs considered for the real dataset calibration

Overlapping pairs		Overlap ratio	Direction
(i)	Strips 1&2	100%	Opposite directions
(ii)	Strips 3&4	100%	Opposite directions
(iii)	Strips 3&5	50%	Same direction
(vi)	Strips 1&6	70%	Opposite directions
(v)	Strips 5&7	50%	Opposite directions
(vi)	Strips 7&8	40%	Opposite directions
(vii)	Strips 2&6	70%	Same direction

Table 7 - Estimated 3D transformation parameters for 7 overlapping strip pairs w.r.t. the local ground coordinate system

Strips	XT (m)	YT (m)	ZT (m)	ω (sec)	φ (sec)	κ (sec)
1&2	-0.25	1.27	-0.01	10.54	1.34	67.68
3&4	-0.01	0.52	0.02	-2.59	-9.72	20.52
3&5	-0.32	-0.19	-0.06	7.20	96.48	6.48
2&6	-0.42	0.15	0.01	-4.65	74.61	-136.10
1&6	-0.67	1.51	-0.06	4.68	91.08	71.64
5&7	-0.13	0.55	0.04	0.68	12.96	-5.40
7&8	0.48	0.82	0.06	1.62	-166.32	-2.84

Table 8 - Biases in the system parameters estimated by the simplified method using the transformation parameters reported in Table 7

δΔX (m)	δΔY (m)	δΔω (sec)	δΔφ (sec)	δΔκ (sec)	Δρ (m)	δS
-0.11	-0.10	86.00	-16.00	41.00	0.28	0.000670

Table 9 - Biases in the system parameters estimated by the quasi-rigorous method using only overlapping strip pairs

δΔX (m)	δΔY (m)	δΔω (sec)	δΔφ (sec)	δΔκ (sec)	Δρ (m)	δS
-0.05	-0.09	84.3	-1.2	32.5	-0.09	0.00103

Table 10 - Biases in the system parameters estimated by the quasi-rigorous method using overlapping strip pairs and the control surface

δΔX (m)	δΔY (m)	δΔω (sec)	δΔφ (sec)	δΔκ (sec)	Δρ (m)	δS
-0.04	-0.03	67.07	-0.87	33.67	-0.06	0.00099

4. CONCLUSIONS AND RECOMMENDATIONS FOR FUTURE WORK

In this paper, new approaches for the estimation of biases in LiDAR system parameters were introduced: the simplified method using overlapping strips and the quasi-rigorous method using time-tagged point coordinates of overlapping strips and trajectory position data. The simplified method requires parallel overlapping LiDAR strips acquired by fixed wing platform over an area with moderate elevation change compared to the flying height. It utilizes only the LiDAR point cloud and the system biases are estimated using the detected discrepancies between overlapping LiDAR strips. The quasi-rigorous method can deal with non-parallel strips and can handle trajectory heading variations and hilly terrain since it makes use of time-tagged point cloud and trajectory position data.

The performance of the developed calibration procedures has been verified using simulated and real datasets. It has been established that the simplified calibration method is not sensitive to reasonable deviations from the presented assumptions. The quasi-rigorous method, on the other hand, shows a good performance regardless of deviations from parallelism in the flight lines. The results using real data have illustrated the feasibility of the proposed calibration procedures in operational environments.

As a future work, we will improve the quasi-rigorous method by considering possible pitch and roll variations in the flight trajectory. In addition, the possibility of eliminating the need for the time-tagged trajectory data will be investigated.

ACKNOWLEDGEMENT

This work was supported by the Canadian GEOIDE NCE Network (SII-72) and the National Science and Engineering Council of Canada (Discovery Grant). The authors would like to thanks LACTEC, UFPR, Brazil for providing the real datasets.

REFERENCES

McGlone, J.C. *Manual of Photogrammetry*, 5th Edition, American Society for Photogrammetry and Remote Sensing, pp. 994-995, 2004.

Ackermann, F. Airborne Laser Scanning - Present Status and Future Expectations, *ISPRS Journal of Photogrammetry & Remote Sensing*, v. 54, n. 2-3, p. 64-67, 1999.

Baltsavias, E.P. Airborne Laser Scanning - Basic Relations and Formulas, *ISPRS Journal of Photogrammetry & Remote Sensing*, v. 54, n. 2-3 p. 199-214, 1999.

Bang, K.I. et al. Integration of Terrestrial and Airborne LiDAR Data for System Calibartion. *The International Archives of the Photogrammetry, Remote Sensing and Spatial Information Sciences*, WG I/2, 3-11 July, Beijing, China, p. 391-398, 2008.

Bretar F. et al. Solving the Strip Adjustment Problem of 3D Airborne Lidar Data, Proceedings of the IEEE IGARSS'04, Anchorage, USA, 20-24 Sep., 2004. [CDROM]

Ghanma, M. Integration of Photogrammetry and LIDAR, Ph.D. Dissertation, Department of Geomatics Engineering, the Univertisy of Calgary, Calgary, Canada, 2006.

Habib, F.A. et al. Automatic Surface Matching for the Registration of LiDAR Data and MR Imagery, *ETRI Journal*, v. 28, n. 2, p. 162-174, 2006.

Habib, F. et al. LiDAR system Self-calibration Using Planar Patches from Photogrammetric Data, *The 5th Inetrnational Symposium on Mobile Mapping Technology*, Padua, Italy, 28-31 May, 2007. [CDROM]

Lee, J. et al. Adjustment of Discrepancies between LiDAR Data Strips Using Linear Features, *IEEE Geoscience and Remote Sensing Letter*, v. 4, n. 3, p. 475-479, 2007.

Morin, K.W. Calibration of Airborne Laser Scanners, M.S. Dissertation, Department of Geomatics Engineering, the Univertisy of Calgary, Calgary, Canada, 2000.

Postolov, Y. et al. Registration of Airborne Laser Data to Surface Generated By Photogrammetric Means, *International Archieve of Photogrammetry and Remote Sensing*, 32(3W13): p. 95-99, 1999.

Schenk, T.Modeling and Analyzing Systematic Errors in Airborne Laser Scanners, *Technical Notes in Photogrammetry*. The Ohio State University, v. 19, 2001.

Skaloud, J.; Lichti, D. Rigorous Approach to Boresight Self-calibration in Airborne Laser Scanning, *ISPRS Journal of Photogrammetry & Remote Sensing*, v. 61, n. 6, p. 47-59, 2006.

Vaughn, C. R. et al. Georeferencing of Airborne Laser Altimeter Measurements, *International Journal of Remote Sensing*, v. 17, n. 11, p. 2185-2200, 1996.

Wehr, A.; Lohr, U. Airborne Laser Scanning - an Introduction and Overview, *ISPRS Journal of Photogrammetry & Remote Sensing*, v. 54, n. 2-3, p. 68-82, 1999.